




Ultrafast active water pump driven by terahertz electric fields

Qi-Lin Zhang ¹, Rong-Yao Yang ², Chun-Lei Wang ^{3,4,5,*} and Jun Hu^{3,4,†}

¹*School of Mathematics-Physics and Finance and School of Materials Science and Engineering, Anhui Polytechnic University, Wuhu 241000, China*

²*School of Physics, Southeast University, Nanjing 211189, China*

³*Zhangjiang Laboratory, Interdisciplinary Research Center, Shanghai Advanced Research Institute, Chinese Academy of Sciences, Shanghai 201210, China*

⁴*Shanghai Institute of Applied Physics, Chinese Academy of Sciences, Shanghai 201800, China*

⁵*College of Science, Shanghai University, Shanghai 20044, China*



(Received 2 June 2022; accepted 7 November 2022; published 28 November 2022)

A highly efficient, easy-to-implement, long-ranged and nondestructive way to realize active pumping has been still a great challenge. Here, using molecular dynamics simulations, terahertz electric field (TEF) is employed to stimulate an active pump for water transportation by bias applied in a (6, 6) single-walled carbon nanotube under no external pressure gradient. An ultrafast conductivity (up to $\approx 9.5 \text{ ns}^{-1}$) through the pump around a characteristic frequency of 14 THz is found. The excellent pumping ability is attributed to the resonance coupling between the TEF and water molecules, in which water molecules can gain considerable energy continuously to break the binding of hydrogen bonds and the spatial symmetry. This proposed TEF-driven pump design will offer a guide in polar molecule transport through artificial or biological nanochannels, particularly in a controllable, noncontact and large-scale process.

DOI: [10.1103/PhysRevFluids.7.114202](https://doi.org/10.1103/PhysRevFluids.7.114202)

I. INTRODUCTION

A unidirectional continuous water transportation through nanochannels, including passive and active transport, is of great significance in many applications such as flow nanosensors [1], drug delivery [2], transmembrane transport [3], nanofiltration [4], and desalination [5]. Usually, the passive water transportation through nanochannels [5–9] is realized by the hydrostatic or osmotic pressure being maintained by a large reservoir. The active transport [10] that broadly exists in biology has great realistic significance and value to develop excellent nanofluidics and regulate biological activities. However, it is still a great challenge to efficiently achieve the artificial active transport at the nanoscale, mainly due to the difficulty of external energy transfer and absorption. In recent years, several active nanopumps have also been engineered by designing systems with vibrating carbon nanotubes [11], rotating carbon nanotube (CNT) [12], rotating electric fields [13], oscillating charges [14], alternating hydrophobicity [15], or dragging mechanism [16] to drive water molecules to transport continuously in single direction. But in all, these prior studies have shown that the spatial asymmetric potential and continuous energy acquisition are two necessary conditions for the operation of a molecular pump [17,18]. Significantly, Netz *et al.* [14] presented a design of molecular water pump by electrodes with oscillating charges in a broad gigahertz frequency range, which demonstrates that time-varying electric field is a good candidate technology to realize a molecular water pump at the nanoscale.

*Corresponding author: wangchunlei@zjlab.org.cn

†Corresponding author: hujun@sinap.ac.cn

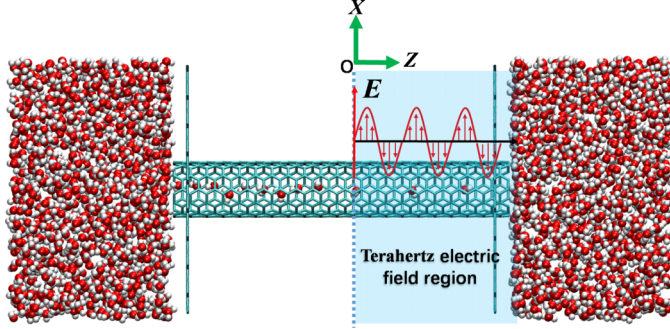


FIG. 1. Snapshot of the simulation system. A 50.34-Å-long (6, 6) SWCNT is perpendicularly embedded into the center holes of two parallel graphene walls with separation vacant space of 46.34 Å. The distance between the bottom end of the SWCNT and the graphene is 2 Å. The red and white balls represent the oxygen and hydrogen atoms of water molecules, respectively. The center of the SWCNT with tube axis aligned along the z direction is located at the origin of the coordinate system. A uniform terahertz electric field is only applied in the $+z$ region (pale blue) along the x direction. The red arrow marked by \mathbf{E} stands for electric field.

Terahertz (THz) technology nowadays has widespread applications in many fields, such as terahertz imaging, environmental monitoring, medical diagnosis, ray astronomy, broadband communication, radar, etc. [19]. This is mainly attributed to the advantages of highly efficient, controllable, long-ranged and nondestructively transmitted terahertz electromagnetic waves [20]. In fact, THz technology has been proven recently to be a strong tool to research protein, aqueous, and ionic solutions, which has also attracted more and more attention in the field of the artificial and biological nanochannels [21–25]. Noticeably, theoretical and experimental studies have shown that the characteristic frequencies of water and biomacromolecules fall in the THz frequency region [26–31]. A series of studies have revealed that THz electrical and THz mechanical vibrations can significantly affect the structure and diffusion coefficient of water inside nanochannels [29–38]. However, according to previous study, uniform application of terahertz electric field (TEF) cannot produce the pumping effect in the absence of a pressure or density gradient in a symmetric channel [17]. It is thus of prime significance for us to first reveal whether and how the TEF drives active transport of water molecules without external pressure gradient.

In this work, we proposed an approach based on the TEF to achieve an active water nanopump by molecular dynamics (MD) simulation. It is found that this nanopump device can be stimulated with an ultrafast and continuous flow by the TEF biasedly applied in a (6, 6) single-walled carbon nanotube (SWCNT). The flux maximum (about 9.5 ns^{-1}), comparable to the flux generated by tens of megabytes of hydrostatic pressure [7,9,39], is more than three times that through the aquaporin-1 channel at a low osmotic pressure [40], and is also one order of magnitude larger than the experimentally measured flux through an SWCNT within 2 nm in diameter under 1 atm pressure gradient [41]. Our findings are helpful for various fluid transport technologies, especially for massive porous materials and complex biochannels. For example, the design is expected to be used in the pumping of polar molecules, transpiration in plants, steam thruster, and so on. Further, it may also be used to regulate the function of proteins being responsible for active transport in animal cells, and open up blocked artificial or biological nanochannels to promote the flow of water or blood.

II. COMPUTATIONAL METHODS

In the present setup, the overall perspective of the pumping system is displayed in Fig. 1. The 50.34-Å-long (6, 6) SWCNT is perpendicularly embedded into the center holes of two parallel graphene walls with a separation vacant space of 46.34 Å. Two water reservoirs are placed at the

ends of the SWCNT. A periodic simulation box of three dimensions is $3.68 \times 3.83 \times 9.9 \text{ nm}^3$ as the replicated unit cell containing 2091 water molecules. The center of the SWCNT with tube axis aligned along the z direction is located at the origin of the coordinate system. All MD simulations are carried out using the large scale MD package NAMD 2.10 [42] in canonical (NVT) ensembles, constant temperature (300 K) being maintained by a Langevin thermostat with a 5-ps^{-1} damping constant. The Chemistry at Harvard Macromolecular Mechanics (CHARMM) [43] force field and TIP3P [44] water model is utilized in all the systems. The CNT-water Lennard-Jones parameters are supposed to be the constant values of $\varepsilon_{\text{cc}} = 0.07 \text{ kcal/mol}$, $\varepsilon_{\text{oo}} = 0.152 \text{ kcal/mol}$, and $\varepsilon_{\text{HH}} = 0.046 \text{ kcal/mol}$, where the cross interaction parameter for carbon, oxygen, and hydrogen complies with the Lorentz-Berthelot mixing criterion. The particle mesh Ewald (PME) method [45] with a multiple time step is used to calculate the electrostatic interaction. Electrostatic and Lennard-Jones interactions are computed by using a smooth (1.0–1.2 nm) cutoff distance. The time step is set to be 1 fs, and the data were recorded every 0.5 ps. The duration of each simulation system is 105 ns: the initial 5 ns was discarded for the system equilibrium, and the last 100-ns samplings were used to analyze the dynamics properties. The molecular graphics program VMD was utilized as a tool for molecular visualization and resultant analysis [46]. All the carbon atoms during the simulations are treated with uncharged and frozen particles at their initial positions for simplicity, as those in Refs. [14,17]. For clarity, the flux is defined as the number difference of water molecules per nanosecond leaving the SWCNT from one end to the opposite end [9,17]. The left ($0 > z \geq -2.5 \text{ nm}$) and right ($0 \leq z \leq 2.5 \text{ nm}$) regions of the SWCNT is denoted by “ $-z$ region” and “ $+z$ region.”

In the present work, all the simulation systems are completely symmetric potential spaces without external pressure gradient, in which water molecules can stochastically transmit in and out of CNTs because of the effect of thermal fluctuation, but no net flux occurs in a long period of time [47]. To induce a net flux, the uniform TEF is only applied in the $+z$ region to break the spatial symmetry of the system, as shown in Fig. 1, which can be realized in practice, e.g., focusing irradiation of TEF [48], inserting the localized electrode device [14], coating nanodevices with metal [49], and wrapping the bionanochannel by the hydrogel for absorption of TEF [50]. With the TEF direction being parallel to the x direction, a periodic electric field force $\mathbf{F}(t)$ (see Fig. S2 in the Supplemental Material [51]), applied on the water molecules, is subjected by

$$\mathbf{F}(t) = q\mathbf{E}(t) = qE_0(\cos(2\pi ft), 0, 0) \quad (1)$$

where q represents the charge of a hydrogen or oxygen atom, t is the time instant, f stands for the frequency of TEF, and E_0 denotes the intensity. Here it should be noted that the strong TEF of order of V/nm generated via, e.g., difference-frequency mixing of two parametrically amplified pulses [52] can drive polar molecular rotations over random thermal motions at room temperature. In this work, unless otherwise denoted, we take the EF intensity $E_0 = 2 \text{ V/nm}$ under which the influence of tunneling ionization can be negligible [34,51,53]. Additionally, because the electric and magnetic fields of the terahertz electromagnetic wave obeys the relation $|E/B| = c$, where c is the speed of light, the magnetic force on water molecules is so small in comparison with the electric force that it is ignored in our simulations [17].

III. RESULTS AND DISCUSSION

MD simulations are performed for the systems under the TEF being applied in the $+z$ region (see Fig. 1) of SWCNT space at different frequencies without external pressure gradient. The flux, with regard to the TEF frequency f , is given in Fig. 2(a), where the flux with average value of zero at $f = 0$ corresponds to the case of zero field ($E_0 = 0 \text{ V/nm}$). Here, the flux is calculated from the last 100-ns simulation average to generate a steady flow. Interestingly, in Fig. 2(a), we can find that the direction and size of the flux are sensitive to the f . It is observed that the flux shows different positive (+flux) and negative (−flux) values at various f , indicating that TEF may drive water through channels in two opposite directions dependence on the f . Further, within the frequency

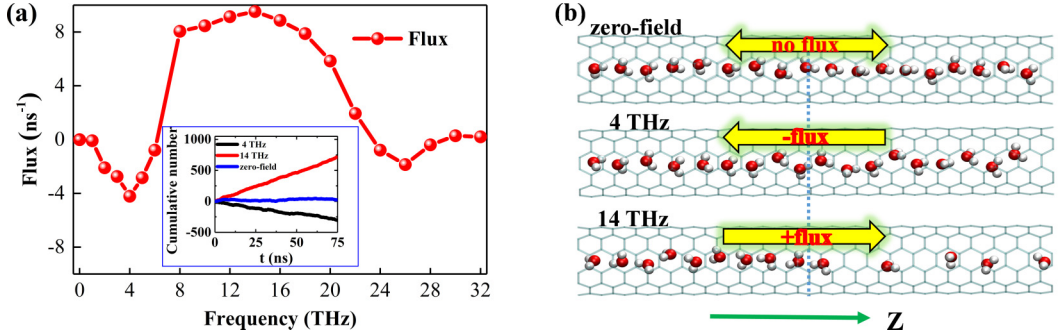


FIG. 2. (a) Relationship of the water flux with the electric field frequency f under the intensity $E_0 = 2$ V/nm. The flux at $f = 0$ corresponds to the case of zero field ($E_0 = 0$ V/nm). Given in the inset is the cumulative number of water molecules with respect to time at zero field, 4 or 14 THz, respectively. (b) Schematic diagram of water molecules through carbon nanotubes at zero field, 4 or 14 THz respectively, where the green arrow represents the z -axis direction.

range of $6 < f < 24$ THz, the +flux means water molecules permeate the SWCNT from left to right (see Supplemental Material Movie S1 [51]). It is also clearly observed that the +flux curve shows a wide peak centered at about 14 THz with a maximum of about 9.5 ns^{-1} , the conductivity of which is several times larger than in previous studies [15,54]. On the contrary, for much lower or higher frequencies, the flux sharply falls off, and an inversion of flux direction happens at $f < 6$ THz or $f > 24$ THz. Figure 2(a) demonstrates that a right-to-left flux (−flux) is generated by TEF stimulus when $1 < f < 6$ THz or $24 < f < 32$ THz (Movie S2 [51]). Note that there are two extreme values of ≈ 4.22 and 1.86 ns^{-1} at around 4 and 26 THz, respectively. Additionally, once beyond the frequency band of $1 < f < 32$ THz, there is no stable flux in Fig. 2(a). These results show that the size and direction of water flow through nanochannels can be easily controlled by the f . To demonstrate the robustness of the above mentioned findings, Fig. 2(a) (inset) shows a rough linear relationship of the cumulative number of water molecules with respect to time at zero field, 4 or 14 THz, indicating that a steady nonflux (blue line), −flux (black line), or +flux (red line) is generated in a long time, respectively. As a visual reference, Fig. 2(b) shows the schematic diagram of water molecules through carbon nanotubes at zero field, 4 or 14 THz, respectively.

To elucidate the detailed mechanism of water unidirectional transport under the TEF, we first investigate the average occupancy number [14,17] of water molecules in the $-z$ region and the $+z$ region of the SWCNT for various f , where the average is taken over the simulation time of statistics. For clarity, we define the average occupancy number of water molecules in the $-z$ region and the $+z$ region of the SWCNT as the symbols N_L^O and N_R^O , respectively. As illustrated in Fig. 3(a), the curves with the blue filled and hollow circles represent N_L^O and N_R^O respectively, where the zero-field result is plotted at $f = 0$. We can observe that the N_R^O curve has a prominent hollow profile in the frequency range of $6 < f < 24$ THz. The curve with red filled circles denotes the density ratios of N_R^O to N_L^O that shows a deep valley around the interval 8–18 THz, where N_R^O is only about half the size of N_L^O . As we know, water molecules can spontaneously diffuse from a high density (N_L^O) to low density (N_R^O) region, and thus the $-z$ region water molecules driven by the density gradient can continuously supply to the $+z$ region in $6 < f < 24$ THz, as shown in the visual reference of 14 THz in Fig. 2(b). It is direct evidence that the density ratio (equivalent density gradient) exhibits an opposite tendency to that of the flux, as comparing Fig. 3(a) with Fig. 2(a). However, when $1 < f < 6$ THz and $24 < f < 32$ THz, although the density ratio gradually decreases until close to 1, surprisingly we still observe the “−flux” take place with two extreme values at 4 and 26 THz in Fig. 2(a). This fact indicates that the direction of flux is not uniquely determined by the density gradient.

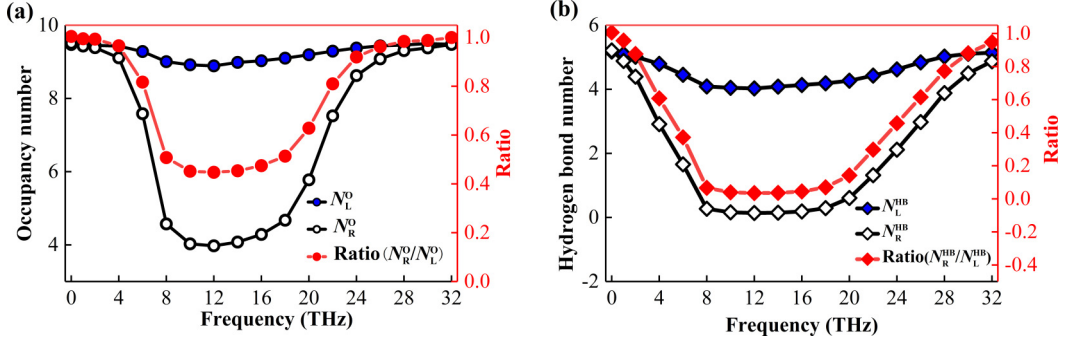


FIG. 3. (a) Average occupancy number of water molecules inside the SWCNT for various electric field frequencies, where the curves with the blue filled (N_L^O) and hollow (N_R^O) circles represent the cases in $-z$ region and $+z$ region, respectively. The curve with red filled circles denotes the density ratios of N_R^O to N_L^O . (b) Average hydrogen-bond (HB) number of water molecules inside the SWCNT for various electric field frequencies, where the curves with the blue filled (N_L^{HB}) and hollow (N_R^{HB}) squares represent the cases in $-z$ region and $+z$ region, respectively. The curve with red filled squares denotes the H-bond ratios of N_R^{HB} to N_L^{HB} .

The outstanding pumping effect is closely associated with the intermolecular structures and interaction of in-tube water molecules. Thus, we also count the average hydrogen bond (HB) number of water molecules inside the SWCNT under the varying frequencies as plotted in Fig. 3(b). The HB is defined in terms of the geometric rule of the O-O distance ≤ 3.5 Å and the bonded O-H...O angle $\leq 30^\circ$ [39,55]. For convenience, we also define the average HB number of water molecules in the $-z$ region and the $+z$ region of the SWCNT as N_L^{HB} and N_R^{HB} , respectively. Figure 3(b) demonstrates that the curves with the blue filled and hollow squares represent N_L^{HB} and N_R^{HB} respectively, where the zero-field result is plotted at $f = 0$. Similar to the occupancy number profile in Fig. 3(a), in the whole frequency range $1 < f < 32$ THz, the N_R^{HB} compared with the N_L^{HB} curve is also dramatically hollow. The curve with red filled squares denotes the HB ratios of N_R^{HB} to N_L^{HB} , which shows a deep and wide valley around the frequency interval 8–18 THz. The dramatic drop of the HB number is associated with the breakage of HBs, due to the absorption of the TEF energy. Previous reports have clearly revealed that the aforesaid phenomenon is ascribed to the strong resonant coupling mechanisms, characterized by librational vibration modes of water molecules [17,33,34] (see Fig. S1 in the Supplemental Material [51]). The 14-THz characteristic frequency in the current study is basically consistent with the previous observations [17,56]. Notably, the N_R^{HB} is almost close to 0 in the broad frequency range 8–18 THz, which indicates that water molecules can acquire enough TEF energy in resonance to completely break the bondage of hydrogen bonds, as shown in Fig. 2(b). The vibration degrees of freedom are therefore markedly increased, which leads to an increase in entropy and a corresponding decrease in free energy [57]. Accordingly, it is observed that the evolution of the flux is inversely proportional to the ratios of average occupancy and HB number of water molecules inside the SWCNT in the resonant frequency region $6 < f < 24$ THz, with the large fluxes corresponding to small occupancy and HB numbers shown in Figs. 2 and 3.

To further understand why the flux direction near the resonance region is opposite, we thus estimated the average kinetic energy E_k of the water molecule along the z -axis direction. Figure 4(a) plots the E_k profiles of simulation systems with zero field (blue), 4 (black), 6 (dark yellow), and 14 THz (red) respectively, where the two vertical dashed lines (pink) denote the positions of the left and right ends of the SWCNT. As shown in Fig. 4(a), the profile of the blue line is approximately a straight line, indicating that the E_k of the water molecule inside and outside the SWCNT is basically equal at zero field. Interestingly, we can observe that the E_k of 14 THz at the $+z$ region (TEF irradiation; see Fig. 1), where the maximum energy barrier difference of about 9 kcal/mol is significantly greater than that at the $-z$ region (non-TEF irradiation). As we know, the temperature of water is mainly determined by the average kinetic energy of water molecules,

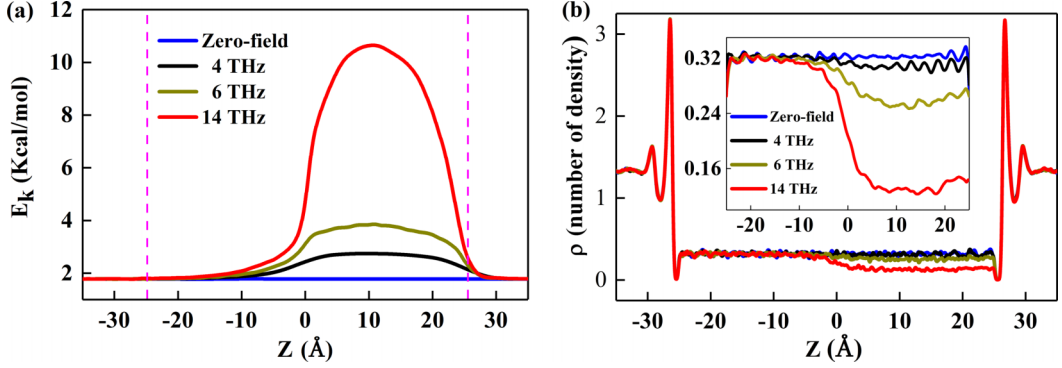


FIG. 4. (a) The average kinetic energy E_k of water molecule as a function of z position for zero field, 4, 6, and 14 THz. The two dashed lines (pink) stand for both ends position of the SWCNT. (b) The average number density ρ distribution profiles of water molecules along the z direction. The window amplification within $-25 < z < 25$ Å is displayed in the inset.

and a rough estimate can be transformed by the equipartition of energy theorem using the relation $E_k = \frac{3}{2}N_A K_B T$, where N_A is the Avogadro constant, K_B is the Boltzmann constant, and T is the temperature. In other words, the kinetic energy gradient is essentially equivalent to a decreasing temperature gradient along the negative direction of the z axis at 14 THz. Intuitively, the flux of 14 THz should be $-\text{flux}$ instead of $+\text{flux}$ in Fig. 2. To understand this counterintuitive behavior, we also estimated the average number density distribution $\rho(z)$ of water molecules along the z direction (see Sec. 5 in the Supplemental Material [51]). As shown in Fig. 4, the density gradient of 14 THz is opposite to the kinetic energy (temperature) gradient. Arguably, whether the flux is $+\text{flux}$ or $-\text{flux}$ is determined by the competition between kinetic energy (temperature) and density gradients of the tube direction. Accordingly, when $6 < f < 24$ THz in Fig. 2(a), the density gradient, over the kinetic energy (temperature) gradient, plays a dominant role in driving water transportation and all the flux presents $+\text{flux}$. As the f becomes gradually further away from the resonance center [17,33], the density and kinetic energy gradient will first tend toward balance, e.g., $f = 6$ THz, so that the suppressed flux reduces to about zero at around 6 and 24 THz [see Fig. 2(a)]. For much lower ($1 < f < 6$ THz) or higher frequencies ($24 < f < 32$ THz), Fig. 3(a) shows that the density ratio is almost close to 1, implying that the density gradient basically disappears. That is, in these frequency ranges, the flux direction is mainly determined by the kinetic energy gradient. As an example, Fig. 4(a) displays that the E_k of 4 THz in the $-z$ region is obviously larger than that in the $+z$ region, whereas the density distributions of the two regions are basically uniform [see Fig. 4(b)]. Thus, the “ $-\text{flux}$ ” is generated along the decreasing direction of the kinetic energy at 4 THz. As it should be, the flow phenomenon generated by the TEF involves the process of convection between different phases of water, the above explanation may not completely reveal the underlying physical mechanism. The in-depth disclosure of the proposed physical hypothesis needs to be further tested and discussed.

In the following, it is worthy to discuss the dependence of water pumping on the TEF intensity E_0 . Fig. 5 shows the water fluxes as a function of the different E_0 at 14 THz. It is found that the flux increases sharply with increasing E_0 from 0.5 to 1.5 V/nm and then basically keeps constant (about 10 ns^{-1}) for $E_0 > 1.5$ V/nm, whereas the flux is almost unaffected when the electrical field intensity E_0 is less than 0.5 V/nm. These results show that water molecules inside the nanochannel are still unavoidably affected by thermal motion at room temperature, but the small intensity TEF cannot provide enough torque to suppress the thermal fluctuations of water molecules [14,34,58] (see Fig. S2 in the Supplemental Material [51]). Additionally, for $E_0 > 1.5$ V/nm, water molecules can completely obey the torque drive of the TEF force which acts like a saturated energy absorption state, so that the fluxes are not significantly different under the higher strength of TEF, for instance, at $E_0 = 2$ or 2.5 V/nm in Fig. 5.

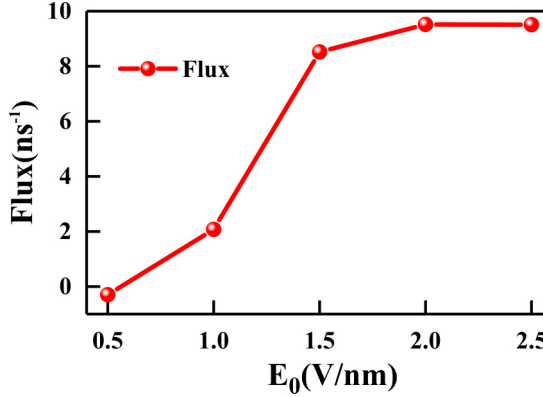


FIG. 5. The flux as a function of different electric field intensity E_0 at 14 THz.

Finally, in order to investigate the application range of THz active water pump, we have performed some additional simulations (see the Fig. S3-S6 in the Supplemental Material [51]). It is found that TEF can also stimulate the unidirectional flow of water in large diameter nanochannel, cyclic peptide nanotubes [59], and confined two-dimensional space. Meanwhile, we also found that the pump effect can be produced by the TEF biased irradiation at different positions of the nanochannels. These results indicate that our proposed designing of active molecular pump based on the TEF technology is quite universal at the nanoscale.

IV. CONCLUSION

To summarize, a new pumping design for manipulating water biased transport through nanochannels in the absence of external pressure gradient is proposed by controlling the frequency of TEF. A series of simulations show that, when the TEF is only partially applied in a symmetrical nanochannel, a steady flow can be excited in a single direction. This active water pump can realize ultrafast conductivity (up to $\approx 9.5 \text{ ns}^{-1}$) and controllable pumping direction by adjusting the frequency of TEF. The key physical mechanism governing the pumping is explained as follows: due to the resonances, arising from librational and translational modes of in-tube water molecules coupling with the TEF, the average kinetic energy, occupancy and HB numbers have changed significantly under the applied THz region. As a result, the system equilibrium is so markedly broken that density and kinetic energy gradients are simultaneously established, resulting in driving a continuous biased flow.

This proposed pumping approach based on the THz technology can take place in a controllable, long-ranged, noncontact and large-scale process, which will provide an innovative idea for the development and design of active water pump in practice. For example, one can design an active pump based on the THz technology for the different candidate nanochannels, including zeolites, nanometer-size porous materials, covalent or metal-organic frameworks [60,61]. Furthermore, this THz-driven design may also open a new avenue to develop possible implications for targeted delivery of molecules or ions in transmembrane channels. For instance, it can be used to simulate adenosine triphosphate (ATP) releasing photons to realize the function of the ion or proton pump in organisms [62].

ACKNOWLEDGMENTS

This work was supported by the National Natural Science Foundation of China (Grants No. 12022508, No. 12074394, and No. 11604001), and overseas and domestic visiting research projects of outstanding young backbone talents in Anhui Universities (Grant No. gxgnfx2020092). The

computing resources were partly provided by the Supercomputer Center of University of Science and Technology of China.

- [1] S. Ghosh, A. K. Sood, and N. Kumar, Carbon nanotube flow sensors, *Science* **299**, 1042 (2003).
- [2] N. Kam, M. O’Connell, J. Wisdom, and H. Dai, Carbon nanotubes as multifunctional biological transporters and near-infrared agents for selective cancer cell destruction, *Proc. Natl. Acad. Sci. USA* **102**, 11600 (2005).
- [3] R. H. Tunuguntla, R. Y. Henley, Y. C. Yao, T. A. Pham, M. Wanunu, and A. Noy, Enhanced water permeability and tunable ion selectivity in sub-nanometer carbon nanotube porins, *Science* **357**, 792 (2017).
- [4] A. Srivastava, O. Srivastava, S. Talapatra, R. Vajtai and P. M. Ajayan, Carbon nanotube filters, *Nat. Mater.* **3**, 610 (2004).
- [5] F. Fornasiero *et al.*, Ion exclusion by sub-2nm carbon nanotube pores, *Proc. Natl. Acad. Sci. USA* **105**, 17250 (2008).
- [6] J. Liu, G. Shi, and H. Fang, Water flow in carbon based nanoporous membranes impacted by interactions between hydrated ions and aromatic rings, *Nanotechnology* **28**, 084004 (2007).
- [7] X. J. Gong, J. Y. Li, H. J. Lu, H. Zhang, R. Z. Wan, and H. P. Fang, Enhancement of Water Permeation Across a Nanochannel by the Structure Outside the Channel, *Phys. Rev. Lett.* **101**, 257801 (2008).
- [8] W. Choi, Z. Ulissi, S. Shimizu *et al.*, Diameter-dependent ion transport through the interior of isolated single-walled carbon nanotubes, *Nat. Commun.* **4**, 2397 (2013).
- [9] F. Zhu, E. Tajkhorshid, and K. Schulten, Theory and simulation of water permeation in aquaporin-1, *Biophys. J.* **86**, 50 (2004).
- [10] R. W. Albers, Biochemical aspects of active transport, *Annu. Rev. Biochem.* **36**, 727 (1967).
- [11] Q. Hu, S. Rong, and W. Guo, Vibrating carbon nanotubes as water pumps, *Nano Res.* **4**, 284 (2011).
- [12] J. Feng, H. Ding, C. Ren *et al.*, Pumping of water by rotating chiral carbon nanotube, *Nanoscale* **6**, 13606 (2014).
- [13] D. Ostler, S. K. Kannam, P. J. Davis, F. Frascoli, and B. D. Todd, Electropumping of water in functionalized carbon nanotubes using rotating electric fields, *J. Phys. Chem. C* **121**, 28158 (2017).
- [14] K. F. Rinne, S. Gekle, D. J. Bonthuis, and R. R. Netz, Nanoscale pumping of water by ac electric fields, *Nano Lett.* **12**, 1780 (2012).
- [15] N. Arai, T. Koishi, and T. Ebisuzaki, Nanotube active water pump driven by alternating hydrophobicity, *ACS Nano* **15**, 2481 (2021).
- [16] P. Král and B. Wang, Material drag phenomena in nanotubes, *Chem. Rev.* **113**, 3372 (2013).
- [17] Q. L. Zhang, R. Y. Yang, W. Z. Jiang, and Z. Q. Huang, Fast water channeling across carbon nanotubes in far infrared terahertz electric fields, *Nanoscale* **8**, 1886 (2016).
- [18] D. J. Bonthuis, D. Horinek, L. Bocquet, and R. R. Netz, Electrokinetics at aqueous interfaces without mobile charges, *Langmuir* **26**, 12614 (2010).
- [19] A. Rostami, H. Rasooli, and H. Baghban, *Terahertz Technology* (Springer, Berlin, 2011).
- [20] W. Tu, S. Zhong, M. Luo, and Q. Zhang, Non-destructive evaluation of hidden defect beneath the multilayer organic protective coatings based on terahertz technology, *Front. Phys.* **9**, 304 (2021).
- [21] P. H. Siegel, Terahertz technology in biology and medicine, *IEEE MTT-S Int. Microwave Symp. Dig.* **52**, 2438 (2004).
- [22] V. Conti Nibali and M. Havenith, New insights into the role of water in biological function: Studying solvated biomolecules using terahertz absorption spectroscopy in conjunction with molecular dynamics simulations, *J. Am. Chem. Soc.* **136**, 12800 (2014).
- [23] W. Bo, L. Guo, Y. Yang, J. Ma, and Y. Gong, Numerical study of voltage-gated Ca^{2+} transport irradiated by terahertz electromagnetic wave, *IEEE Access* **8**, 10305 (2020).
- [24] K. Wu, C. Qi, Z. Zhu, C. Wang, B. Song, and C. Chang, Terahertz wave accelerates DNA unwinding: A molecular dynamics simulation study, *J. Phys. Chem. Lett.* **11**, 7002 (2020).

- [25] Y. Li, C. Chang, Z. Zhu, L. Sun, and C. Fan, Terahertz wave enhances permeability of the voltage-gated calcium channel, *J. Am. Chem. Soc.* **143**, 4311 (2021).
- [26] C. C. Yu, K. Y. Chiang, M. Okuno, T. Seki, and Y. Nagata, Vibrational couplings and energy transfer pathways of water's bending mode, *Nat. Commun.* **11**, 5977 (2020).
- [27] S. T. Van DerPost *et al.*, Strong frequency dependence of vibrational relaxation in bulk and surface water reveals sub-picosecond structural heterogeneity, *Nat. Commun.* **6**, 8384 (2015).
- [28] J. E. Boyd, A. Briskman, V. L. Colvin, and D. M. Mittleman, Direct Observation of Terahertz Surface Modes in Nanometersized Liquid Water Pools, *Phys. Rev. Lett.* **87**, 147401 (2001).
- [29] K. Johnson, Terahertz vibrational properties of water nanoclusters relevant to biology, *J. Biol. Phys.* **38**, 85 (2012).
- [30] M. Heyden, J. Sun, S. Funkner, G. Mathias, H. Forbert, M. Havenith, and D. Marx, Dissecting the THz spectrum of liquid water from first principles via correlations in time and space, *Proc. Natl. Acad. Sci. USA* **107**, 12068 (2010).
- [31] R. Y. Yang, Z. Q. Huang, S. N. Wei, Q. L. Zhang, and W. Z. Jiang, The resonant heating of heavy water solutions under the terahertz pulse irradiation, *J. Mol. Liq.* **229**, 148 (2017).
- [32] M. Ma, F. Grey, L. Shen, M. Urbakh, S. Wu *et al.*, Water transport inside carbon nanotubes mediated by phonon-induced oscillating friction, *Nat. Nanotechnol.* **10**, 692 (2015).
- [33] Q. L. Zhang, W. Z. Jiang, J. Liu, R. D. Miao, and N. Sheng, Water Transport Through Carbon Nanotubes with the Radial Breathing Mode, *Phys. Rev. Lett.* **110**, 254501 (2013).
- [34] Z. Zhu, C. Chang, Y. Shu, and B. Song, Transition to a superpermeation phase of confined water induced by a terahertz electromagnetic wave, *J. Phys. Chem. Lett.* **11**, 256 (2019).
- [35] Z. Zhu, C. Chen, C. Chang, and B. Song, Terahertz-light induced structural transition and superpermeation of confined monolayer water, *ACS Photonics* **8**, 781 (2021).
- [36] P. K. Mishra, V. Bettaque, O. Vendrell, R. Santra, and R. Welsch, Prospects of using high-intensity THz pulses to induce ultrafast temperature-jumps in liquid water, *J. Phys. Chem. A* **122**, 5211 (2018).
- [37] J. Kou, H. Lu, F. Wu, J. Fan, and J. Yao, Electricity resonance-induced fast transport of water through nanochannels, *Nano Lett.* **14**, 4931 (2014).
- [38] J. Kou, J. Yao, H. Lu, B. Zhang *et al.*, Electromanipulating water flow in nanochannels, *Angew. Chem. Int. Ed.* **54**, 2351 (2015).
- [39] Q. L. Zhang, R. Y. Yang, Fast transport of water molecules across carbon nanotubes induced by static electric fields, *Chem. Phys. Lett.* **644**, 201 (2016); Q. L. Zhang, Y. X. Wu, R. Y. Yang, J. L. Zhang, and R. F. Wang, Effect of the direction of static electric fields on water transport through nanochannels, *ibid.* **762**, 138139 (2021).
- [40] M. L. Zeidel *et al.*, Ultrastructure, pharmacologic inhibition, and transport selectivity of aquaporin channel forming integral protein in proteoliposome, *Biochemistry* **33**, 1606 (1992).
- [41] J. K. Holt, H. G. Park, Y. Wang, M. Stadermann *et al.*, Fast mass transport through sub-2-nanometer carbon nanotubes, *Science* **312**, 1034 (2006).
- [42] C. J. Phillips *et al.*, Scalable molecular dynamics with NAMD, *J. Comput. Chem.* **26**, 1781 (2005).
- [43] A. D. MacKerell *et al.*, All-atom empirical potential for molecular modeling and dynamics studies of proteins, *J. Phys. Chem. B* **102**, 3586 (1998).
- [44] W. L. Jorgensen, J. Chandrasekhar, J. D. Madura, R. W. Impey, and M. L. Klein, Comparison of simple potential functions for simulating liquid water, *J. Chem. Phys.* **79**, 926 (1983).
- [45] T. A. Darden, D. M. York, and L. G. Pedersen, Particle mesh Ewald: An N-log (N) method for Ewald sums in large systems, *J. Chem. Phys.* **98**, 10089 (1993).
- [46] W. Humphrey, A. Dalke, and K. Schulten, VMD: Visual molecular dynamics, *J. Mol. Graphics* **14**, 33 (1996).
- [47] R. Wan, H. Lu, J. Li, J. Bao, J. Hu, and H. Fang, Concerted orientation induced unidirectional water transport through nanochannels, *Phys. Chem. Chem. Phys.* **11**, 9898 (2009).
- [48] T. Milda, I. Simonas, T. Vincas, M. Linas, U. Andrzej, R. Gediminas *et al.*, Focusing of terahertz radiation with laser-ablated antireflective structures, *IEEE Trans. Terahertz Sci. Technol.* **8**, 541 (2018).
- [49] A. E. Hughes, I. S. Cole, T. H. Muster, and R. J. Varley, Designing green, self-healing coatings for metal protection, *NPG Asia Mater.* **2**, 143 (2010).

- [50] Y. Guo, J. Bae, Z. Fang, P. Li, and G. Yu, Hydrogels and hydrogel-derived materials for energy and water sustainability, *Chem. Rev.* **120**, 7642 (2020).
- [51] See Supplemental Material at <http://link.aps.org/supplemental/10.1103/PhysRevFluids.7.114202> for two movies and a supplemental document.
- [52] A. Sell, A. Leitenstorfer, and R. Huber, Phase-locked generation and field-resolved detection of widely tunable terahertz pulses with amplitudes exceeding 100 MV/cm, *Opt. Lett.* **33**, 2767 (2008); T. Seifert, S. Jaiswal, M. Sajadi *et al.*, Ultrabroadband single-cycle terahertz pulses with peak fields of 300 kV cm⁻¹ from a metallic spintronic emitter, *Appl. Phys. Lett.* **110**, 252402 (2017).
- [53] A. Ghalgaoui, L. M. Koll, B. Schütte, B. P. Fingerhut, and T. Elsaesser, Field-induced tunneling ionization and terahertz-driven electron dynamics in liquid water, *J. Phys. Chem. Lett.* **11**, 7717 (2020).
- [54] X. Gong, J. Li, H. Lu, R. Wan, and H. Fang, A charge-driven molecular water pump, *Nat. Nanotechnol.* **2**, 709 (2007).
- [55] Y. Lu and J. Chen, Adjustable diffusion enhancement of water molecules in a nanoscale water bridge, *Nanoscale* **13**, 1000 (2021).
- [56] L. Thrane, R. H. Jacobsen, P. Uhd Jepsen, and S. R. Keiding, THz reflection spectroscopy of liquid water, *Chem. Phys. Lett.* **240**, 330 (1995).
- [57] T. A. Pascal, W. A. Goddard, and Y. Jung, Entropy and the driving force for the filling of carbon nanotubes with water, *Proc. Natl. Acad. Sci. USA* **108**, 11794 (2011).
- [58] Y. W. Guo, J. Y. Qin, J. H. Hu, J. H. Cao, Z. Zhu, and C. L. Wang, Molecular rotation-caused autocorrelation behaviors of thermal noise in water, *Nucl. Sci. Tech.* **31**, 53 (2020).
- [59] J. Liu, J. Fan, M. Tang, M. Cen, J. Yan, Z. Liu *et al.*, Water diffusion behaviors and transportation properties in transmembrane cyclic hexa-, octa- and decapeptide nanotubes, *J. Phys. Chem. B* **114**, 12183 (2010).
- [60] X. Liu, H. Pang, X. Liu, Q. Li, N. Zhang *et al.*, Orderly Porous Covalent Organic Frameworks-based Materials: Superior Adsorbents for Pollutants Removal from Aqueous Solutions, *Innovation* **2**, 100076 (2021).
- [61] Y. W. Hao, S. Pang, X. Q. Zhang, and L. Jiang, Quantum-confined superfluid reactions, *Chem. Sci.* **11**, 10035 (2020).
- [62] F. Zhang, B. Song, and L. Jiang, The quantized chemical reaction resonantly driven by multiple MIR-photons: From nature to the artificial, *Nano Res.* **14**, 4367 (2021).